Excited state and charge dynamics of hybrid organic/inorganic heterojunctions. I. Theory

C. Kyle Renshaw[1] and Stephen R. Forrest[1,2,3]

[1]*Department of Physics, University of Michigan, Ann Arbor, Michigan 48109, USA*

[2]*Department of Electrical Engineering and Computer Science, University of Michigan, Ann Arbor, Michigan 48109, USA*

[3]*Department of Materials Science and Engineering, University of Michigan, Ann Arbor, Michigan 48109, USA*

(Received 27 April 2014; published 9 July 2014)

The different cohesive forces that bond organic (i.e. excitonic) and inorganic semiconductors lead to widely disparate dielectric constants, charge mobilities, and other fundamental optoelectronic properties that make junctions between these materials interesting for numerous practical applications. Yet, there are no detailed theories addressing charge and energy transport across interfaces between these hybrid systems. Here, we develop a comprehensive physical model describing charge transport and photocurrent generation based on first-principles charge and excited state dynamics at the organic/inorganic heterojunction. We consider interfaces that are trap-free, as well as those with an exponential distribution of trap states. We find that the hybrid charge-transfer state resulting from photon absorption near the junction that subsequently migrates to the heterointerface is often unstable at room temperature, leading to its rapid dissociation into free charges that are collected at the device contacts. In the companion Paper II [A. Panda *et al.*, Phys. Rev. B **90**, 045303 (2014)], we apply our theories to understanding the optical and electronic properties of archetype organic/inorganic heterojunction diodes. Our analysis provides insights for developing high performance optoelectronic devices whose properties are otherwise inaccessible to either conventional excitonic or inorganic semiconductor junctions.

DOI: 10.1103/PhysRevB.90.045302 PACS number(s): 73.40.−c, 78.66.−w, 81.05.Fb

I. INTRODUCTION

The classical description of inorganic semiconductors based on charge recombination at, and diffusion to *p-n* junctions has resulted in the so-called "ideal diode", or Shockley equation [1] that, with many subsequent extensions and modifications, has served as the foundation of semiconductor device physics over the past six decades. More recently, Giebink *et al.* have extended this analysis to include excitonic semiconductors [2,3], a large and important class of materials exemplified by organic materials now achieving widespread use in a range of electronic and optical applications [4]. The differences in properties between organic and inorganic semiconductors that ultimately originate from their vastly different bond energies (i.e. organics are physically bonded by weak van der Waals forces, whereas inorganic semiconductors are chemically bonded by a combination of covalent and ionic forces) require a significantly different physical description. For example, inorganic semiconductors are characterized by their hardness, ready formation of crystalline structures, a high charge mobility ($\mu \sim$ 10–10 000 cm^2/V-s) and dielectric constant ($\varepsilon \sim$10–100), and the ability to be doped to increase conductivity by several orders of magnitude [5]. In contrast, excitonic materials tend to be relatively soft, forming a range of crystalline, nanocrystalline, and amorphous morphologies, have low mobility [6,7] ($\mu \sim 10^{-6}$–5 cm^2/V-s) and dielectric constant [8] ($\varepsilon \sim$ 1.5–4), and have low conductivities even when doped [9,10]. Furthermore, the low carrier mobilities of organic materials results in charge self-trapping, thereby generating high effective mass "polarons" [11], whereas the low effective mass of inorganics leads to extensive delocalization of charge [12]. Hence, the dynamics of excitons (i.e. excited states) and charges demand a different physical description than that developed by Shockley.

Intermediate between pure excitonic and inorganic semiconductors is the combination of these two materials, forming a hybrid organic/inorganic heterojunction (OI-HJ) at their point of contact. Indeed, many promising technologies employ OI-HJs as their charge-separating interface, including OI photodiodes [13] and solar cells [14,15], dye-sensitized solar cells (DSSCs) [16,17], colloidal quantum dot solar cells and light emitting devices [18–20], and nanoparticle/organic solar cells [21]. Furthermore, there have been numerous recent studies of hybrid polaritons and other structures that have potential for use in lasers, and in the study of nonlinear optical phenomena such as hybrid polaritons in optical microcavities [22–25]. Finally, metal oxide semiconductor-organic thin film heterojunctions are finding widespread application in high intensity, stacked organic light emitting devices (OLEDs) and tandem organic photovoltaic (OPV) cells, and hence their detailed characterization is essential for their optimization [26–28].

While there have been many examples of devices that exploit OI-HJs, a comprehensive understanding of their influence on charge generation, recombination, and extraction has yet to be developed. Previous models have primarily relied on an "equivalent circuit" description of the HJs to model their current density versus voltage (*J-V*) characteristics, both in the dark and under illumination [29,30]. These models have variously considered the organic-inorganic contacts to be equivalent to Schottky-type metal-semiconductor junctions [31,32] or more accurately as HJs [29,30,33]. While they give a reasonable phenomenological description of the observed characteristics, they fail to provide a fundamental physical understanding of the dynamics of hybrid state formation and dissociation that governs the properties of the OI-HJ.

In this paper, we derive a first-principles physical model that describes the dynamics of charge and excited state transport

to the interface of the hybrid OI-HJ. The model is based on the injection and photogeneration of charge in the inorganic semiconductor and Frenkel excitons in the organic layer that migrate to the interface where a hybrid charge transfer exciton (HCTE) is formed. The HCTE is analogous to a polaron-pair state (i.e. a charge transfer state spanning the heterojunction) at an excitonic junction. The HCTE then rapidly dissociates into free charges. The HCTE is a coulombically bound charge pair at the heterointerface; however, unlike the case of polaron-pairs where both charge species are localized, in the HCTE, the charge in the inorganic is delocalized over many lattice ions, while the polaron on the organic is localized on only one or a few molecules.

The model is developed for an n-P anisotype Type II staggered [5] OI-HJ. Here, n refers to the majority carrier type of the inorganic semiconductor. The P implies that the position of the Fermi energy is below the center of the organic energy gap and hence is closer to the highest occupied molecular orbital (HOMO) as compared to its position relative to the lowest unoccupied MO (LUMO).

The diode characteristics are dominated by interface recombination at low current and by the carrier transport properties of the contacting semiconductors at higher currents. The model is general, in that it can be easily modified for application to isotype junctions (e.g. n-N and p-P) as well as to Type I (nested) HJ energy level offsets. These generalizations are treated in the Appendix. The analysis leads to a rigorous description of the J-V characteristics of the hybrid structure, both in the dark and under illumination. At low currents (corresponding to reverse bias or at small forward voltage), we observe ideal diode behavior reminiscent of both Shockley p-n and excitonic junctions. At high currents, the diode characteristics are dominated by space-charge effects due to transport through the low mobility organic semiconductor, as previously observed by Forrest *et al.* [14,29,30].

In the companion Paper II [34], we apply the model to the specific cases of hybrid devices utilizing a thin-film inorganic TiO_2 layer that is relevant to DSSCs [35], and InP that is useful in solar cells and photodetectors [13,15]. The HJ between an inorganic metal-oxide and an organic semiconductor also plays an important role as a charge generation layer in OLEDs and as a buffer layer for hole extraction in OPVs [26,27,36].

This paper is organized as follows: The theory of OI-HJs is described in Sec. II. Specifically, Sec. II.A details the physical processes that occur at the OI heterointerface under near-equilibrium (i.e. low voltage and current) conditions. The dynamics of charge carriers and HCTE states are included in the current model describing an "ideal" n-P junction. We intentionally exclude the effects of charge extraction barriers, injection barriers, or bulk recombination that can be considered using procedures analogous to those employed in describing nonidealities in inorganic and excitonic junctions. Section II.B combines calculations of the electric field distribution with interfacial charge recombination to obtain the charge density and voltage distribution across the contacting layers under nonequilibrium (i.e. high voltage and current) conditions. Section III applies these results to an example pentacene/n-Si OI-HJ and details its implications on the open circuit voltage of OI-HJ photovoltaic cells. We close this section with a brief comparison of the diode equations for inorganic, excitonic, and OI-HJs. Conclusions are presented in Sec. IV. In the Appendix, we extend the model to several different OI-HJs where both carrier type and relative energy level offset arrangements are different from the n-P OI-HJ.

II. THEORY OF CONDUCTION FOR ORGANIC/INORGANIC HETEROJUNCTIONS

In Fig. 1(a), we show an n-P OI-HJ in the absence of interface defects or traps. In neglecting deep traps, we ignore loss due to trapped charge recombination, which is equivalent to assuming defect states at the inorganic surface are inactive or nonexistent. Indeed, it has been shown that in some cases, the presence of the organic layer can passivate the inorganic surface [15,37,38]. Nevertheless, there is also ample evidence

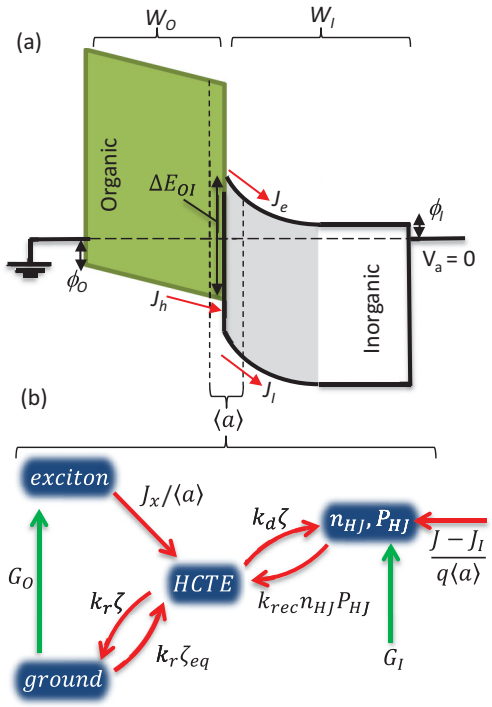

FIG. 1. (Color online) (top) Equilibrium energy level diagram for a hybrid organic/inorganic n-P heterojunction. The depletion region formed in the inorganic is indicated in gray and has a width of W_I. The Fermi level in the inorganic is at ϕ_I below the conduction band edge. The organic layer thickness is W_O, and ϕ_O is the barrier for injecting holes into the organic highest occupied molecular orbital from the anode. The interface energy gap is $\Delta E_{\rm OI}$. Charge generation and recombination at the interface occurs in a region of width $\langle a \rangle$ around the interface according to the state diagram (bottom panel). Excitons from the organic dissociate at a rate $J_X/\langle a \rangle$ to form HCTEs. The HCTE recombines and dissociates at rates k_r and k_d, respectively. Carriers at the interface ($n_{\rm HJ}$ electrons in the inorganic and $P_{\rm HJ}$ holes in the organic) recombine to form HCTEs and are populated by current flowing to the interface. Minority carriers generated in the inorganic are extracted through the organic and populate $P_{\rm HJ}$ at a rate $J_I/q\langle a \rangle$. Here, J_I is the current density from holes that are photogenerated in the inorganic and subsequently extracted through the organic. Here, J_e is the electron current density in the inorganic and $J_h = J$ is the hole current density flowing in the organic.

that in other cases, interface states play a dominant role in determining the photoresponse [15] of the OI-HJ. Hence, this latter case which may be an intrinsic property of the hybrid junction will also be considered below.

Photocarrier generation can occur via three mechanisms: (i) direct band-to-band absorption of a photon in the inorganic semiconductor that results in minority carrier diffusion to the OI-HJ with an interface energy gap of $\Delta E_{\rm OI}$ [see Fig. 1(a)], or (ii) photon absorption in the organic leading to exciton generation and diffusion to the junction (with an exciton current of J_X), or (iii) direct absorption by the HCTE state at the OI-HJ [39]. In the first two cases, once the photoexcited species migrates to the HJ, a HCTE state forms by Coulomb attraction across the interface. Since the third case usually has a very low absorption cross-section and hence is unlikely to play a significant role in the OI-HJ optoelectronic properties, we do not consider it in the subsequent discussion The HCTE is a generally unstable precursor to bimolecular recombination to the ground state or, alternatively, to dissociation by generating free charge at the OI heterojunction ($n_{\rm HJ}$, $P_{\rm HJ}$) in the inorganic and organic layers, respectively. Figure 1(b) shows the interface state diagram for the processes leading to charge generation. The free carriers $n_{\rm HJ}$ and $P_{\rm HJ}$ are captured at a rate of $k_{\rm rec} n_{\rm HJ} P_{\rm HJ}$ to form HCTEs at density ζ and with a characteristic diameter between the electron and polaron $\langle a \rangle$ across the interface, thereby defining the "active interfacial volume". The corresponding rate equations for ζ,$n_{\rm HJ}$ and $P_{\rm HJ}$ as functions of time t are given by

$$\frac{d}{dt}\zeta = -k_r(\zeta - \zeta_{\rm eq}) - k_d\zeta + k_{\rm rec} n_{\rm HJ} P_{\rm HJ} + \frac{J_X}{\langle a \rangle} = 0, \qquad (1)$$

$$\frac{d}{dt} n_{\rm HJ} = -k_{\rm rec} n_{\rm HJ} P_{\rm HJ} + k_d\zeta + \frac{J_e}{q\langle a \rangle} = 0, \qquad (2)$$

and

$$\frac{d}{dt} P_{\rm HJ} = -k_{\rm rec} n_{\rm HJ} P_{\rm HJ} + k_d\zeta + \frac{J_h - J_I}{q\langle a \rangle} = 0, \qquad (3)$$

where the final equality holds for steady-state conditions. Here, q is the electronic charge, k_r and k_d are the rates that HCTEs recombine to the ground state and dissociate into free carriers, respectively. The thermal generation rate of HCTEs is $k_r\zeta_{\rm eq}$, where $\zeta_{\rm eq}$ is their equilibrium density given by $\zeta_{\rm eq} = k_{\rm rec} n_{\rm HJ,eq} P_{\rm HJ,eq}/k_{d,\rm eq}$. Equilibrium corresponds to an external voltage $V_a = 0$ in the absence of illumination. Tables I and II provide definitions and values of all major variables used.

Minority carriers photogenerated in the inorganic must be extracted through the organic layer and populate $P_{\rm HJ}$ at a rate J_I. Also, J_e and J_h are the electron current in the inorganic and the hole current in the organic, respectively. Typically in organic materials, their large bandgap and significant asymmetries in the mobilities of electrons and holes suggests that the current is primarily carried by only one charge species. In our case, we assume that the hole density and mobility are much greater than the electron density and mobility in the organic (which is the case for the specific organic films considered in Paper II [34]), and hence $J_h \equiv J$, although this theory is easily modified for an electron current in the organic that is comparable to or greater than J_h. Continuity demands that $\nabla \cdot J = 0$ everywhere in steady-state. At the interface, this implies that $J_e + J_I = J_h \equiv J$. Hence, Eqs. (2) and (3) are identical, resulting in perfect coupling between $n_{\rm HJ}$ and $P_{\rm HJ}$.

TABLE I. Definitions of variables used.

Variable		Definition	
Organic	Inorganic	Layer properties	Units
$P_{\rm HJ}$	$n_{\rm HJ}$	Carrier density at the OI interface	$\rm cm^{-3}$
P_c	n_c	Carrier density at the contact	$\rm cm^{-3}$
V_O	V_I	Voltage across each layer	V
δ_O	δ_I	Fraction of voltage dropped across each layer	–
qJ_X	J_I	Photocurrent generated by each layer	$\rm A/cm^2$
W_O	W_I	Active layer thickness	cm
ϕ_O	ϕ_I	Injection barrier at the contacts	eV
Q_O	Q_I	Net space-charge accumulated (or depleted)	$\rm cm^{-2}$
$E_{f,p}$	$E_{f,n}$	Quasi-Fermi level for holes and electrons	eV
a_O	a_I	Width of HCTE in each layer	cm
		Interface Properties	
$\langle a \rangle$		Characteristic width of HCTE at the OI interface	cm
$\langle \varepsilon_r \rangle$		HCTE effective permittivity	F/cm
ζ		HCTE density	$\rm cm^{-3}$
E_B		HCTE binding energy	eV
$\Delta E_{\rm OI}$		Interface energy gap at the OI heterojunction	eV
η		HCTE dissociation efficiency	–
k_r,k_d		HCTE recombination and dissociation rate	$\rm s^{-1}$
$k_{\rm rec}$		Bimolecular recombination rate	$\rm cm^3 \cdot s^{-1}$
$V_a[V_{\rm bi}]$		Applied [built-in] voltage	V

TABLE II. Values of parameters used in model OI-HJ calculations.

Organic [inorganic]	Definition	Value	Units
$\varepsilon_O[\varepsilon_I]$	Dielectric permittivity	0.35[1.05]	pF/cm
$\mu_O[\mu_I]$	Hole [electron] mobility	10^{-4}[1500]	$\rm cm^2/Vs$
$E_{g,O}[E_{g,I}]$	Bandgap energy	2.1 [1.12]	eV
$E_{\rm LUMO}[E_c]$	Electron affinity	2.8 [4.05]	eV
$E_{\rm HOMO}[E_v]$	Ionization energy	4.9 [5.17]	eV
$N_{\rm HOMO}[N_v]$	HOMO [valence band] effective DOS	$10^{21}[9.8 \times 10^{18}]$	$\rm cm^{-3}$
$N_{\rm LUMO}[N_c]$	LUMO [conduction band] effective DOS	$10^{21}[2.8 \times 10^{19}]$	$\rm cm^{-3}$
$P_D[N_D]$	Doped carrier density	$10^{14}[10^{16}]$	$\rm cm^{-3}$
$H_O[H_I]$	Characteristic trap density	$10^{18}[10^{18}]$	$\rm cm^{-3}$
$T_{t,O}[T_{t,I}]$	Characteristic trap temperature	600 [2000]	$\rm cm^{-3}$
$W_O[W_I]$	Active layer thickness	20 [1000]	nm
$\phi_O[\phi_I]$	Injection barrier into the organic [inorganic]	0.2 [0.2]	eV
$a_O[a_I]$	Radius of the HCTE in the organic [inorganic]	1[6]	nm
m^*	HCTE effective mass	$0.19m_0$	kg
k_r	HCTE recombination rate	10^9	$\rm s^{-1}$

In steady-state, the rate equations can be solved to eliminate ζ. Hence, the current is given by

$$J = q\langle a\rangle k_{\rm rec}(1-\eta_d)\left(n_{\rm HJ}P_{\rm HJ} - \frac{k_d}{k_{d,\rm eq}}n_{\rm HJ,eq}P_{\rm HJ,eq}\right) - J_{\rm ph}, \tag{4}$$

where $J_{\rm ph} = qJ_X\eta_d - J_I$ is the total photocurrent which is the sum of the exciton current generated in the organic and the direct carrier generation current in the inorganic. Also, $J_I < 0$ by convention and $J_X > 0$, resulting in $J_{\rm ph} > 0$. Also, $\eta_d = k_d/(k_d + k_r)$ is the HCTE dissociation efficiency.

Although bound HCTE states have been experimentally detected at ZnO/polymer [40] and CdTe/polymer [41] interfaces, due to the high dielectric constant and delocalized nature of carriers in the inorganic semiconductor, the HCTE binding energy E_B is expected to be much smaller than that for polaron pairs characteristic of purely excitonic heterojunctions [2]. Indeed in some cases, $E_B/k_BT \leqslant 1$ such that the interface exciton may be unstable or at best metastable (i.e. characterized by a very short lifetime $\sim$ picoseconds) at room temperature. Here, k_B is the Boltzmann constant and T is temperature. To estimate E_B, the HCTE can be thought of as a hybrid between a Frenkel and Wannier-Mott exciton bound to the heterojunction, as illustrated in Fig. 2(a). In this example, the hole is localized to within $\sim$1 nm the interface; while the electron tunnels into the inorganic, extending $\sim$6 nm over many atomic sites. The charge comprising the exciton rapidly dissociates into an electron on the inorganic semiconductor conduction band that is bound to the hole polaron localized at the OI-HJ, thereby forming the HCTE. The HCTE then dissociates either by thermal excitation or by the internal junction field that forces the electron to drift toward the bulk, freeing the hole polaron from the interface. The dynamical properties of the HCTE are also strongly dependent on whether the transfer is between energetically resonant or nonresonant states at the two sides of the junction [22].

While this is an admittedly oversimplified semiclassical picture of the coupled state bound at the interface that can only be accurately understood from a full quantum mechanical description, it nevertheless provides a useful starting point for understanding the charge transfer process.

Following Onsager theory, the critical radius [42] for the hole in the HCTE is $r_c = q^2/4\pi\langle\varepsilon_r\rangle k_BT$, corresponding to the separation at which the Coulombic interaction is equal to k_BT. Here, $\langle\varepsilon_r\rangle$ is the dielectric permittivity given by $\langle\varepsilon_r\rangle = (a_I\varepsilon_I + a_O\varepsilon_O)/(a_I + a_O)$ where $\varepsilon_I(\varepsilon_O)$ is the permittivity of the inorganic (organic) layer, and $a_I(a_O)$ is the extent of the HCTE into the inorganic (organic) layer. To estimate E_B as a function of $\langle\varepsilon_r\rangle$, we use the Bohr model [12,43] to approximate the radius of the HCTE as

$$\langle a\rangle = a_I + a_O = \frac{8\pi\langle\varepsilon_r\rangle\hbar^2}{m^*q^2}, \tag{5}$$

where the reduced effective mass is $m^* = (1/m_I + 1/m_O)^{-1}$, $m_I(m_O)$ is the effective mass of the inorganic (organic) layer, and $\hbar$ is Planck's constant divided by 2π. Note that, typically, the electron mass in the inorganic is much less than the hole mass in the organic. This corresponds to a binding energy of

$$E_B = \frac{q^2}{8\pi\langle a\rangle\langle\varepsilon_r\rangle}. \tag{6}$$

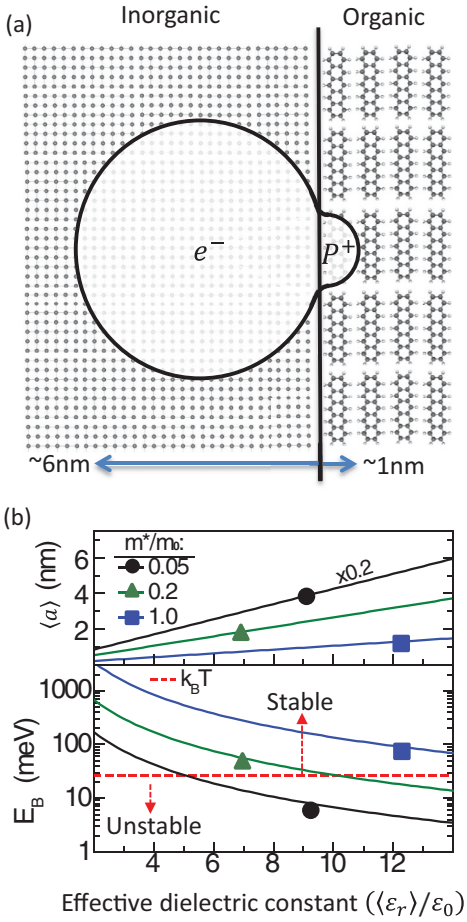

FIG. 2. (Color online) (a) Conceptual illustration of the HCTE state. The electron in the inorganic is delocalized over a large number of lattice sites due to the relatively large dielectric screening, similar to the case of a Wannier-Mott exciton. This electron is Coulombically bound to a positive polaron (hole) in the organic that is localized on one or two molecules at the interface, analogous to a Frenkel state. The arrows at the bottom note typical extent of these states into the respective materials. (b) Binding energy E_B and characteristic radius $\langle a\rangle$ of an exciton as a function of effective dielectric constant according to the theory in the text. Here, E_B and $\langle a\rangle$ are plotted for the effective mass $m^* = 1m_0, 0.2m_0$, and $0.05m_0$. The dashed line indicates the thermal energy at room temperature k_BT that demarks regions of HCTE stability $E_B > k_BT$ and instability $E_B < k_BT$. Here, $\langle\varepsilon_r\rangle$ is the relative dielectric permittivity and ε_0 is the permittivity of free space.

Figure 2(b) shows the exciton binding energy and characteristic exciton radius as functions of the effective dielectric constant for electron effective masses of $m^* = 1m_0, 0.2m_0$, and $0.05m_0$ (typical of the range for inorganics), where m_0 is the mass of a free electron. This model assumes that the electronic states are extended and that a localized electron is formed by a wave packet whose motion can be characterized by the effective mass m^*. The direct extension of m^* to disordered organics is not rigorous, but it has been estimated that, for most small molecule crystalline organic semiconductors, m^* ranges from $0.2m_0$ to $10m_0$, depending on how tightly adjacent molecules are stacked [44–46]. However,

this semiclassical approximation is not expected to be accurate for large effective masses and highly localized charges; a rigorous calculation of the binding energy once again requires a fully quantum mechanical approach.

For convenience, we assume that the field dependence of the dissociation rate of the HCTE state is described by the Onsager-Braun (OB) [42,47] model, viz.

$$k_d = A_{\mathrm{OB}} k_{\mathrm{rec}} \exp\left(-\frac{E_B}{k_B T}\right) \frac{J_1\left[2\sqrt{-2b}\right]}{\sqrt{-2b}} \equiv k_{d,0} \frac{J_1\left[2\sqrt{-2b}\right]}{\sqrt{-2b}}. \tag{7}$$

Here, J_1 is the first-order Bessel function, $b = q^3 F_{\mathrm{HJ}}/8\pi\langle\varepsilon_r\rangle k_B^2 T^2$, F_{HJ} is the electric field at the interface on the organic side of the HJ, and $k_{d,0}$ is the HCTE dissociation rate at $F_{\mathrm{HJ}} = 0$. This model is valid for low mobility semiconductors where the mean free path is much less than r_c. In the case of a single mobile carrier considered here, the field dependence of k_d may be larger than that predicted by OB, yet it nevertheless serves as a first-order approximation. The prefactor A_{OB}^{-1} is assumed to be the volume of an ion pair of radius $\langle a\rangle$ [47], i.e. $A_{\mathrm{OB}} = 3/4\pi\langle a\rangle^3$. In the case where the HCTE is expected to have a partial Wannier-Mott character, we use $A_{\mathrm{OB}} = (m^* k_B T/3\pi\hbar^2)^{3/2}$ where m^* is the effective mass of the electron in the inorganic semiconductor.

The bimolecular recombination rate for low mobility solids is diffusion-limited, and therefore follows Langevin recombination statistics where $k_{\mathrm{rec}} = q\langle\mu\rangle/\langle\varepsilon_r\rangle$, with an effective mobility of $\langle\mu\rangle = \mu_I + \mu_O$ [47]. In the case of a highly mobile electron in the inorganic semiconductor, $k_{\mathrm{rec}} = v_{\mathrm{th}}\sigma$, where $v_{\mathrm{th}} = \sqrt{3k_B T/m^*}$ is the thermal velocity of the electron and $\sigma = \pi r_c^2$ is its trap capture cross-section. Here, we assume that electric field screening in the high-dielectric constant inorganic semiconductor allows for neglect of the effects of the electrostatic potential [48] on the capture rate.

A. Current conduction under quasi-equilibrium conditions

If J is sufficiently small so that the electron and hole quasi-Fermi levels ($E_{f,n}$ and $E_{f,p}$) are flat throughout the respective inorganic and organic layers, then the interface carrier densities are given by

$$n_{\mathrm{HJ}} = N_c \exp\left(-\frac{\phi_I}{k_B T}\right) \exp\left(\frac{qV_I}{k_B T}\right) = n_c \exp\left(\frac{qV_I}{k_B T}\right), \tag{8}$$

and

$$P_{\mathrm{HJ}} = N_{\mathrm{HOMO}} \exp\left(-\frac{\phi_O}{k_B T}\right) \exp\left(\frac{qV_O}{k_B T}\right) = P_c \exp\left(\frac{qV_O}{k_B T}\right). \tag{9}$$

Here, N_{HOMO} and N_c are the effective densities of states of the HOMO of the organic and at the conduction band minimum of the inorganic, ϕ_O and ϕ_I are the injection barriers into the organic (from the anode) and inorganic (from the cathode) shown in Fig. 1(a), and V_O and V_I are the voltages dropped across the organic and inorganic layers, respectively. In the case of a thick inorganic layer where the depletion width does not extend to the contacts, then $\phi_I = E_c - E_{f,n}$ in the undepleted equilibrium region. Here, E_c is the energy of the conduction band minimum and $E_{f,n}$ is the electron quasi-Fermi level. In this case, n_c is the electron density at equilibrium as determined by the ionized dopant density N_D. Also, P_c is the hole density in the organic at the anode contact. Note that due to the low organic layer conductivity, an equilibrium region comparable to that in the inorganic layer does not exist, i.e. the entire organic layer is depleted of free carriers, and hence the field across it is uniform.

Using these definitions and following procedures analogous to Giebink *et al.* [2], we obtain from Eqs. (4), (8) and (9)

$$J = q\langle a\rangle k_{\mathrm{rec}} N_{\mathrm{HOMO}} N_c (1-\eta_d) \exp\left(-\frac{\Delta E_{\mathrm{OI}}}{k_B T}\right) \times \left(\exp\left(\frac{qV_a}{k_B T}\right) - \frac{k_d}{k_{d,\mathrm{eq}}}\right) - J_{\mathrm{ph}}. \tag{10}$$

Here, $\Delta E_{\mathrm{OI}} = V_{\mathrm{bi}} + \phi_O + \phi_I$ as defined in Fig. 1(a), and V_{bi} is the built-in voltage determined by the inorganic Fermi level and the anode work function (modified by energy level shifts, such as those due to interface dipoles) [49]. The applied voltage is related to the voltage dropped across each layer and the built-in voltage using $V_a = V_O + V_I + V_{\mathrm{bi}}$.

Next, we consider the case where the organic film contains a high density of trapped charge. The traps can have an extrinsic source (such as morphological defects and impurities), although in organics they also have an intrinsic origin due to variations in molecular conformations and configurations. Often, the intrinsic trap density of states is assumed to be exponential and is described by

$$P_t = H_O \exp\left(\frac{E_{\mathrm{HOMO}} - E_{f,p}}{k_B T_{t,O}}\right) = H_O \left(\frac{P}{N_{\mathrm{HOMO}}}\right)^{1/l_O}. \tag{11}$$

The trap density H_O, the characteristic trap temperature $T_{t,O}$, and the normalized trap temperature $l_O = T_{t,O}/T$ can be used to fully describe the trap distribution in the organic film. This treatment is valid for disordered organic films that lack a sharp band edge due to disorder-induced transport level broadening [6,50]. Indeed, in organic films, the conduction level density of states itself is often treated by an exponential distribution of site energies, or as a Gaussian distribution that is approximated by an exponential near the energies of the frontier orbitals. For generality, we use a similar trap profile near the inorganic conduction band minimum, defined by the parameters H_I, $T_{t,I}$, and l_I. This approximation has been shown to be a suitable distribution for disordered inorganics [51,52]. In principle, however, the ensuing analysis applies to any trap distribution, and we will also discuss the case for crystalline inorganics that are typically characterized by a discreet trap level where $n_t = H_I \exp(-\frac{E_c - E_{f,n} - E_t}{k_B T})$, and E_t is the trap energy [5,53].

We assume that interface recombination is dominated by the recombination of a free carrier with a trapped charge,

where

$$J = q\langle a\rangle(1-\eta_d)\left[k_{\mathrm{rec},n}\left(n_{\mathrm{HJ}}P_{\mathrm{HJ},t} - \frac{k_d}{k_{d,\mathrm{eq}}}n_{\mathrm{HJ},\mathrm{eq}}P_{\mathrm{HJ},t,\mathrm{eq}}\right) + k_{\mathrm{rec},p}\left(n_{\mathrm{HJ},t}P_{\mathrm{HJ}} - \frac{k_d}{k_{d,\mathrm{eq}}}n_{\mathrm{HJ},t,\mathrm{eq}}P_{\mathrm{HJ},\mathrm{eq}}\right)\right] - J_{\mathrm{ph}}, \tag{12}$$

Here, $k_{\mathrm{rec},n}$ and $k_{\mathrm{rec},p}$ are the recombination rates for a free electron with a trapped hole or a free hole with a trapped electron, respectively. Further, $P_{\mathrm{HJ},t}$ and $n_{\mathrm{HJ},t}$ are the trapped carrier densities at the HJ and can be determined using Eq. (11). This expression assumes that $n_{\mathrm{HJ}}P_{\mathrm{HJ},t}$ and $n_{\mathrm{HJ},t}P_{\mathrm{HJ}}$ are greater than either $n_{\mathrm{HJ},t}P_{\mathrm{HJ},t}$ or $n_{\mathrm{HJ}}P_{\mathrm{HJ}}$, such that J is dominated by free carrier recombination with trapped carriers. Using Eqs. (5) and (6), the current is

$$J = q\langle a\rangle(1-\eta_d)\left[k_{\mathrm{rec},n}N_cH_O\exp\left(-\frac{\alpha_O}{k_BT}\right)\left(\exp\left(\frac{qV_a}{n_Ok_BT}\right) - \frac{k_d}{k_{d,\mathrm{eq}}}\right) + k_{\mathrm{rec},p}N_{\mathrm{HOMO}}H_I \times \exp\left(-\frac{\alpha_I}{k_BT}\right)\left(\exp\left(\frac{qV_a}{n_Ik_BT}\right) - \frac{k_d}{k_{d,\mathrm{eq}}}\right)\right] - J_{\mathrm{ph.}} \tag{13}$$

Here,

$$\alpha_O = \frac{\Delta E_{\mathrm{OI}}}{n_O} + \frac{l_O-1}{l_O}(\delta_O\phi_I - \delta_I\phi_O), \tag{14}$$

$$\alpha_I = \frac{\Delta E_{\mathrm{OI}}}{n_I} + \frac{l_I-1}{l_I}(\delta_I\phi_O - \delta_O\phi_I), \tag{15}$$

$$n_O = \frac{l_O}{\delta_I(l_O-1)+1}, \tag{16}$$

and

$$n_I = \frac{l_I}{\delta_O(l_I-1)+1}. \tag{17}$$

Now $\delta_O = V_O/(V_a - V_{\mathrm{bi}})$ and $\delta_I = V_I/(V_a - V_{\mathrm{bi}})$ are the fractions of the applied voltage dropped across the respective organic and inorganic layers, respectively. Contrary to the trap-free case, the voltage distribution across the layers affects the current even in the near-equilibrium approximation used here. This is important due to the asymmetry of the electronic properties of the organic and inorganic layers (see Sec. II.B). Note that in the case of discrete traps in the inorganic semiconductor, Eq. (15) must be modified such that $\alpha_I = E_t$.

If the HCTE binding energy is small compared to k_BT (which can occur at high T and/or for high ε_I), the bound state is readily dissociated, resulting in a large k_d. In the limit that $E_B/k_BT \to 0$, the HCTE is coupled to the bath of free carriers, such that $k_d = k_{\mathrm{rec}}/A_{\mathrm{OB}}$ is a constant, and $\zeta \approx A_{\mathrm{OB}}n_{\mathrm{HJ},\mathrm{eq}}P_{\mathrm{HJ},\mathrm{eq}} + J_X/k_d\langle a\rangle$. In this case, Eqs. (2) and (3) reduce to

$$\frac{dn_{\mathrm{HJ}}}{dt} = -k_{\mathrm{rec}}(n_{\mathrm{HJ}}P_{\mathrm{HJ}} - n_{\mathrm{HJ},\mathrm{eq}}P_{\mathrm{HJ},\mathrm{eq}}) + \frac{qJ_X + J - J_I}{q\langle a\rangle} = 0, \tag{18}$$

with a similar expression for $P_{\mathrm{HJ.}}$ As expected, this is equivalent to the absence of HCTEs, where the excitons immediately dissociate into free carriers that subsequently recombine to the ground state.

Following the above analysis, for the trap-free case, we simply obtain

$$J = q\langle a\rangle k_{\mathrm{rec}}N_{\mathrm{HOMO}}N_c\exp\left(-\frac{\Delta E_{\mathrm{OI}}}{k_BT}\right) \times \left[\exp\left(\frac{qV_a}{k_BT}\right) - 1\right] - J_{\mathrm{ph}}, \tag{19}$$

and for an exponential trap distribution

$$J = q\langle a\rangle\left\{k_{\mathrm{rec},n}N_cH_O\exp\left(-\frac{\alpha_O}{k_BT}\right)\left[\exp\left(\frac{qV_a}{n_Ok_BT}\right) - 1\right] + k_{\mathrm{rec,p}}N_{\mathrm{HOMO}}H_I\exp\left(-\frac{\alpha_I}{k_BT}\right)\left[\exp\left(\frac{qV_a}{n_Ik_BT}\right) - 1\right]\right\} - J_{\mathrm{ph}}. \tag{20}$$

These expressions are nearly identical to Eqs. (10) and (13), although they are independent of HCTE dissociation dynamics and ultimately are the limiting case where HCTEs dissociate with an efficiency $\eta_d \to 1$. Note that $k_{\mathrm{rec}}(1-\eta_d)$ reduces to $A_{\mathrm{OB}}k_r$ in the limit that $k_d = k_{\mathrm{rec}}/A_{\mathrm{OB}} \gg k_r$.

Now, defining a saturation current density of $J_S = q\langle a\rangle k_{\mathrm{rec}}N_{\mathrm{HOMO}}N_c\exp(-\Delta E_{\mathrm{OI}}/k_BT)$, then Eq. (19) simplifies to the familiar form of the ideal diode equations analogous to those derived by Shockley [1] and Giebink *et al.* [2]

$$J = J_S\left[\exp\left(\frac{qV_a}{k_BT}\right) - 1\right] - J_{\mathrm{ph}}. \tag{21}$$

In a similar fashion, an interface with traps yields the current

$$J = \left\{J_{\mathrm{SO}}\left[\exp\left(\frac{qV_a}{n_Ok_BT}\right) - 1\right] + J_{\mathrm{SI}}\left[\exp\left(\frac{qV_a}{n_Ik_BT}\right) - 1\right]\right\} - J_{\mathrm{ph}}, \tag{22}$$

making the appropriate substitutions for the saturation currents for the organic, J_{SO}, and inorganic semiconductors, J_{SI}, by comparison with Eq. (20).

B. Current conduction under nonequilibrium conditions

The voltage distribution in the device becomes important when a high density of traps are present at the interface or when the small current approximation is no longer valid. For example, it has been found that at high forward voltages, the OI-HJ current is typically limited by space charge effects in the organic [29]. In this case, the high current regime is reached at the voltage when the space charge current [e.g. $J = (9/8)(\varepsilon_O\mu_OV^2/d^3)$ for the trap-free case [50,54]] is equal to that of Eq. (19).

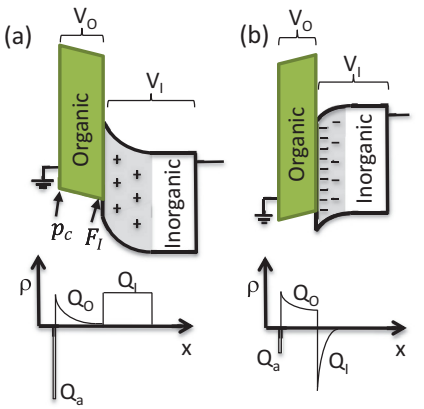

FIG. 3. (Color online) (a) Schematic of a n-P OI-HJ under low or reverse bias ($V_a < V_{\rm bi}$, where V_a and $V_{\rm bi}$ are the applied and built-in voltages, respectively). The n-type inorganic is in depletion mode resulting in a positive space-charge Q_I. The organic is reverse biased; hence, the electric field sweeps holes out of the organic layer resulting in a low charge density Q_O and uniform field in the organic layer. Excess charge Q_a depleted from the inorganic layer is accumulated at the anode-organic interface. (b) Forward bias condition for the OI-HJ. Electrons accumulate in the inorganic at the OI-HJ such that $Q_I < 0$. The electric field is oriented to force injection of holes into the organic layer that accumulate at the OI-HJ, resulting in a large Q_O. The charge in the anode is determined by charge conservation, i.e. $Q_a = -(Q_I + Q_O)$.

Due to the radically different electrical properties (i.e. mobility and carrier concentration) of the organic and inorganic layers, we expect the voltage distribution to be asymmetric under applied voltages and currents that are large, i.e. that are far from equilibrium. To determine the voltage distribution which sets the ratio δ_O/δ_I from Eqs. (14)–(17), we must first understand the distribution of charge across all of the layers and contacts. Coupling this electrostatic solution with the dynamical model for the interface then provides a complete, semiclassical picture for conduction across OI-HJs under all practical bias conditions.

As noted above, organic films are typically undoped, and even when they are intentionally doped, the maximum free carrier concentration rarely exceeds two orders of magnitude above the adventitious (background) concentration of the as-grown organic [55,56]. As a result, the existence of a background carrier density is due to unintentional doping, such as by chemical impurities or oxygen incorporation [57,58], and is expected to be relatively small. For example, for an organic film with a background hole density of $P_D = 10^{15}$ cm^{-3} and $V_{\rm bi} = 0.5$ V (of which half is dropped across the organic), the depletion width [5] is $W_O = \sqrt{2\varepsilon_O(V_{\rm bi}/2)/qP_D} \approx 300$ nm, i.e. larger than the thickness of a typical organic film used in an OI-HJ. With this in mind, the organic layer is assumed to be fully depleted for $V_a < 0$. The resulting energy level diagrams and charge distributions across the OI-HJ under both reverse and forward bias are schematically illustrated in Figs. 3(a) and 3(b), respectively. These are similar to the distributions in a conventional metal-insulator-semiconductor device [5], where we have replaced the "perfect" insulator with a leaky, hole-conducting organic semiconductor.

The voltage dropped across the inorganic layer V_I results in a net space charge Q_I given by [5]

$$Q_I = \mp\sqrt{2k_BTq\varepsilon_I}\sqrt{p_c\left[\exp\left(-\frac{qV_I}{k_BT}\right)+\frac{qV_I}{k_BT}-1\right]+n_c\left[\exp\left(\frac{qV_I}{k_BT}\right)-\frac{qV_I}{k_BT}-1\right]}, \tag{23}$$

where $p_c = N_v\exp[-(E_{\rm g,I}-\phi_I)/k_BT]$ is the equilibrium minority carrier (hole) density in the inorganic, N_v is the valence band effective density of states in the inorganic, and $E_{\rm g,I}$ is its bandgap energy. Under forward bias, $V_I > 0$, and the second exponential dominates, resulting in electron accumulation at the OI heterointerface. Under moderate reverse bias, $V_I < 0$, such that $n_c \cdot qV_I/k_BT$ dominates, thus resulting in charge depletion. Under large reverse bias $V_I \ll k_BT/q \cdot \ln(n_c/p_c) \sim 1.5$ V, the first exponential dominates, corresponding to carrier inversion. This regime is not reached because the limited hole conductivity of the organic allows the injected charge to be extracted by the contacts before a sufficient voltage is established.

The space-charge in the inorganic results in an electric field at the OI-HJ on the organic side given by

$$F_{\rm HJ} = -\frac{Q_I}{\varepsilon_O}, \tag{24}$$

where we have used the Poisson equation $\nabla \cdot F = n/\varepsilon_O$ in the inorganic and $\nabla \cdot (\varepsilon F) = 0$ across the OI-HJ. To ensure that the electric field vanishes at the anode, charge conservation implies that $F_{\rm HJ}$ is terminated by the charge in the organic layer Q_O and/or a sheet charge Q_a induced at the organic/anode interface. Hence, $Q_I + Q_O + Q_a = 0$.

Under reverse bias ($V_a < V_{\rm bi}$), holes are swept out of the organic layer so that a uniform field approximation can be used. Consequently, $F_{\rm HJ}$ is terminated primarily by sheet charge induced at the anode, and the organic behaves as an insulator that capacitively couples the anode to the inorganic semiconductor. In contrast, under forward bias, the electrons accumulate at the OI interface thereby drawing holes into and electrostatically doping the organic layer. The induced hole density can be large, resulting in space-charge screening of the electric field across the layer.

To determine the voltage distribution, we solve the drift-diffusion equation, viz.

$$J = q\mu_O PF - qD\nabla P, \tag{25}$$

with

$$\nabla \cdot F = \frac{q(P-P_D)}{\varepsilon_O}. \tag{26}$$

Here, μ_O is the hole mobility in the organic, and D is its diffusivity. In the absence of intentional doping, the background carrier density P_D is negligible compared to the electrically injected carrier density (i.e. the electrostatic doping level) required to reach thermodynamic equilibrium when the organic contacts both the adjacent inorganic semiconductor and the metal contact. The electrostatic doping profile is determined by the organic material properties, energy level alignments, J, and $V_O(x)$. Equations (25) and (26) are subject to the boundary conditions $F(W_O) = F_{\rm HJ}$ and $P(0) = P_c = N_{\rm HOMO}\exp(-\phi_a/k_BT)$, where W_O is the organic layer thickness, the OI-HJ is located at $x = W_O$, and P_c is the hole density in the organic at the anode contact located at $x = 0$. It is useful to assume that μ_O is independent of electric field and is given by $D = \mu_O k_B T/q$.

When J is small but nonzero, Eqs. (25) and (26) can be solved within the framework of the depletion model [5] by utilizing the resulting analytical electric field profile. Without such a profile, the solution is given by complex Airy functions or by a conditionally convergent power series. Their complexity suggests that numerical simulations of the drift-diffusion equation is a more practical route to calculating the OI-HJ J-V characteristics under nonequilibrium conditions. Numerical simulation also eliminates the need for many explicit assumptions about μ_O, D, and P_D.

Under significant departures from equilibrium, expressions for $P_{\rm HJ}$ and $n_{\rm HJ}$ given by Eqs. (8) and (9) are no longer valid. That is, when $|J| \gg 0$, the quasi-Fermi level is no longer flat, in which case the hole density at the interface is given by

$$P_{\rm HJ} = P_c \exp\left(\frac{qV_O - \Delta E_{f,p}}{k_BT}\right), \tag{27}$$

where $E_{f,p}(x)$ is the local hole quasi-Fermi level, and $\Delta E_{f,p} = E_{f,p}(W_O) - E_{f,p}(0)$ is the total change across the organic film determined by

$$\Delta E_{f,p} = \frac{J}{\mu_O}\int_0^{W_o}\frac{1}{P(x)}dx. \tag{28}$$

Solution of Eq. (28) requires knowledge of $P(x)$ obtained from the numerical solution of the coupled drift-diffusion and Poisson equations described above. The current is then obtained from Eqs. (10) and (13) using the transformation $V_a \to V_a - \Delta E_{f,p}$, or it can be calculated from the carrier densities using Eqs. (4) and (12).

Thus far, we have only discussed the implications of $J \neq 0$ with respect to the organic layer. In contrast, the majority carrier quasi-Fermi level in inorganic semiconductors is always assumed to be flat, i.e. it changes by a negligible amount throughout the depletion region. The reason for the difference between the treatment of the quasi-Fermi levels for organic and inorganic layers is evident from Eq. (28), where $\Delta E_{f,p}$ depends inversely on carrier density and mobility. While the background carrier density in organic films is low, P in Eq. (28) includes doping due to the electrically injected carriers which depends on ϕ_O, V_O, and J. Indeed, local electrically induced doping is often comparable to or larger than carrier densities in doped inorganic layers. Instead, the quasi-Fermi level gradient in the organic [29] results from mobilities that are $10^3 - 10^8$ times lower than in crystalline inorganic semiconductors.

III. RESULTS AND DISCUSSION

A. Open circuit voltage of organic/inorganic heterojunctions

As OI-HJs often find application in solar cells [15,28], it is interesting to determine the device open circuit voltage ($V_{\rm OC}$) in the cases of both stable [$E_B > k_BT$; Eqs. (10) and (13)] and unstable [$E_B < k_BT$; Eqs. (19)–(22)] HCTEs. Here, $V_{\rm OC}$ is determined by setting $J = 0$ in the presence of a photocurrent, with $J_{\rm ph} \gg J_S$.

In the case of the stable HCTE, the derivation of the open circuit voltage is analogous to that of an excitonic junction as described by Giebink *et al.* [2] That is, the trap-free case is based on Eq. (10), viz.

$$qV_{\rm OC} = \Delta E_{\rm OI} - k_BT\ln\left(\frac{k_r}{k_r + k_d}\frac{q\langle a\rangle N_{\rm HOMO}N_c k_{\rm rec}}{J_{\rm ph}}\right). \tag{29}$$

Substituting Eqs. (5) and (7) in the low field limit, which is consistent with $V_a = V_{\rm OC}$, and assuming $k_d \gg k_r$, we have

$$qV_{\rm OC} = \Delta E_{\rm OI} - E_B - k_BT\ln\left(\frac{1}{2}\frac{q^3 N_{\rm HOMO}N_c k_r}{4\pi\langle\varepsilon_r\rangle E_B A_{\rm OB}J_{\rm ph}}\right). \tag{30}$$

For trap-mediated recombination, one of the exponentials in Eq. (13) is usually dominant at high currents. In the case where the first exponential is dominant and assuming that the contact potentials are equal (i.e. $\phi_O \approx \phi_I$), we have

$$qV_{\rm OC} \approx \Delta E_{\rm OI} - n_O E_B - n_O k_BT \times \ln\left(\frac{1}{2}\frac{q^3 H_O N_c k_r}{4\pi\langle\varepsilon_r\rangle E_B A_{\rm OB}J_{\rm ph}}\right). \tag{31}$$

If the second exponential in Eq. (13) is dominant, the subscripts O and I are reversed and $N_c \to N_{\rm HOMO}$. Thus, while the binding energy of the HCTE is smaller than that of excitonic junctions, it nevertheless can lead to a decrease in $V_{\rm OC}$ as T is increased since it appears in the argument of the logarithm, along with the related variables of $\langle\varepsilon_r\rangle$ and $A_{\rm OB}$ (and hence the effective mass m^*). The treatment for an unstable exciton is nearly identical; although, in this case, $E_B \ll k_BT$, and the second term in Eq. (30) vanishes. Hence,

$$qV_{\rm OC} = \Delta E_{\rm OI} - n_O k_BT\ln\left(\frac{k_r}{k_r + k_d}\frac{q\langle a\rangle N_{\rm HOMO}N_c k_{\rm rec}}{J_{\rm ph}}\right). \tag{32}$$

Ultimately, $V_{\rm OC}$ depends on the recombination rate, k_r, of the HCTE. The probability of recombination in OI-HJs, however, is significantly lower than in fully excitonic junctions. In OI-HJs, the internal field at the interface rapidly separates charges following migration to the interface (i.e. $k_d \gg k_r$); hence, there is little opportunity for reactions at rate k_r in Fig. 1(b). Thus, the maximum open circuit voltage as $T \to 0$ is $qV_{\rm OC}^{\rm max} \approx \Delta E_{\rm OI} - nE_B$, independent of the details of morphology or other factors that influence $V_{\rm OC}$ in excitonic junctions [2].

B. Modeling the optoelectronic characteristics of an archetype OI-HJ

We apply the theory in Sec. II to simulate the field distributions and J-V characteristics of an example hybrid pentacene/Si OI-HJ shown in Fig. 4(a). For these calculations, we use the material properties listed in Table II. The resulting J-V characteristics in the trap-free case are shown in Fig. 4(b) in the dark and under illumination as a function of temperature. This device is characterized by a diode behavior that rolls off at high currents due to space-charge effects in the organic. Note that at low forward bias, there is a single exponential increase of J with V.

The characteristics under illumination assume balanced charge generation of $qJ_X = J_I = 1$ mA/cm^2 at the interface. This results in unity dissociation of the bound HCTE, yielding a saturated photocurrent at $V_a < 0.2$ V. In addition, under reverse bias the J-V characteristics are nearly saturated, which

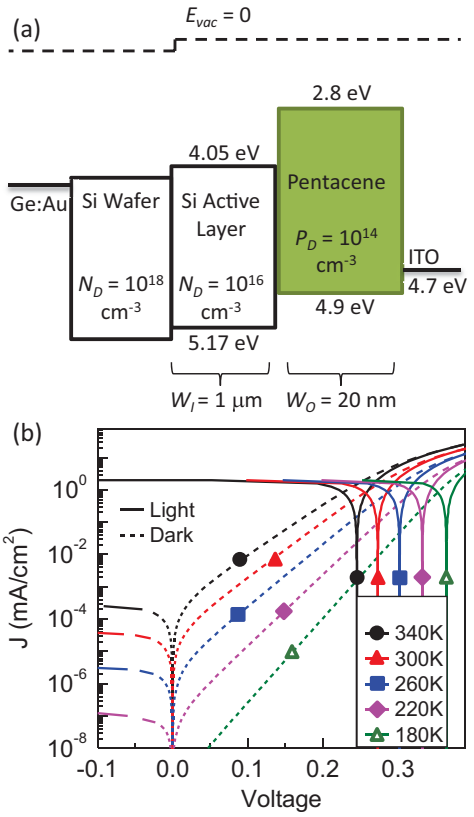

FIG. 4. (Color online) (a) Energy level diagram of an archetype pentacene/Si n-P OI-HJ. The Si active layer is $W_I = 1$ μm thick and is doped at $N_D = 10^{16}$ cm^{-3}. The pentacence layer is $W_O = 20$ nm thick and has a low P-type background doping of $P_D = 10^{14}$ cm^{-3}. The anode contact is assumed to be transparent [i.e. consisting of a transparent conducting oxide such as indium tin oxide (ITO)]. A zero vacuum level (E_{vac}, dashed line) offset between the organic and inorganic indicates there is no interface dipole at the heterojunction. (b) Dark (dashed lines) and illuminated (solid lines) current density versus voltage J-V characteristics of the OI-HJ at different temperatures. The simulations assume a trap-free interface and an illumination that produces $J_I = qJ_X = 1$ mA/cm^2, where J_I is photocurrent generated by the inorganic and qJ_X is Frenkel exciton flux from the organic layer to the organic/inorganic interface.

also differs from the excitonic junction due to the instability of the HCTE that almost immediately ionizes upon formation. In the excitonic case, the tightly bound Frenkel state requires significant field to force its ionization, hence resulting in a small increase in J with increasing reverse bias.

The energy band diagrams, charge, and field distributions are shown in Fig. 5 at various current densities under forward bias. Note that, under reverse and low forward bias (and hence, small J), the frontier orbital (HOMO and LUMO) energies in the organic have a nearly constant slope, indicating that the uniform field approximation is indeed valid. However, under large forward bias (corresponding to large J), a significant density of charge is injected into the film, resulting in a nonuniform field and curvature in the frontier orbital energies. In this case, the large current leads to a pronounced slope in the quasi-Fermi level across the organic layer, characteristic of nonequilibrium conditions.

If traps lead to significant recombination in either layer, the current is given by Eq. (20), and the ideality factor is no longer unity. The trap temperature characterizes the depth that trap states penetrate into the energy gap; for example, $T_{t,O}$ increases with disorder that broadens the density of trap states. These energy gap states result in statistics similar to that of Shockley-Read-Hall recombination. In Fig. 6(a), we show the effect of traps in the J-V characteristics at various temperatures for $H_O = H_I = 10^{18}$ cm^{-3}, $T_{t,O} = 600$ K, and $T_{t,I} = 2000$ K. Here, we observe an inflection in the forward characteristics at low temperatures that is reminiscent of excitonic junctions but clearly departs from expectations for a conventional p-n junction described by the Shockley equation. Figure 6(b) shows the temperature dependence of n_O at various $T_{t,O}$. The increase in ideality factor with increasing $T_{t,O}$ and decreasing ambient temperature is also analogous to that observed for fully excitonic junctions [2], but the ideality factor is significantly smaller in the case of OI-HJs due to the larger voltage drop across the inorganic layer [c.f. Eq. (13)].

In Fig. 7(a), we plot the dark J-V characteristics as a function of the ratio of the HCTE recombination to its dissociation rate $R = k_r/k_{d,0}$, which is varied from 1 to 10^{-6}. It is assumed that HCTE dissociation is very efficient due to its low binding energy along with the comparatively high electron mobility characteristic of inorganic semiconductors. Using values in Table II, Eq. (7) suggests that the HCTE dissociation rate is $k_d \sim 10^{13}$ s^{-1}, which is much larger than the natural singlet exciton recombination rate of $k_r \sim 10^9$ s^{-1}. Indeed, the HCTE recombination rate is reasonably expected to be in the range of $R = 10^6$ s^{-1} to 10^{12} s^{-1} and may vary significantly for different material combinations. As expected, the reverse dark current scales linearly with k_r; the higher recombination rates result in an increase in the rate of charge excitation from the ground state into the various transport bands [c.f. Fig. 1(b)].

While k_d follows Eq. (7), we assume that k_r is independent of electric field. In this case, Fig. 7(b) shows the HCTE dissociation efficiency η_d as a function of electric field for various values of R. We observe that HCTE dissociation is very efficient except for large k_r or large forward bias (corresponding to $F > 0$) where the electric field opposes carrier dissociation. Figure 7(c) shows the reduction in η_d at low temperatures, and η_d reaches 100% at a low reverse-bias

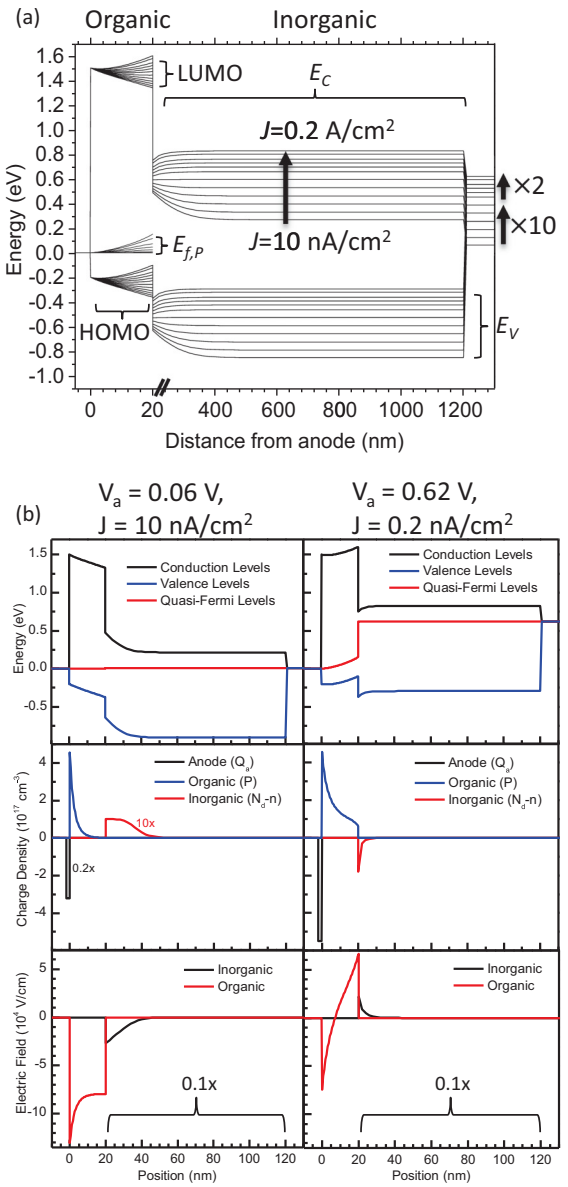

FIG. 5. (Color online) (a) Energy band diagram for the OI-HJ. The valence band E_V and HOMO energy and conduction band E_C and LUMO energy levels are shown for the inorganic and organic layers. The anode contact is shown at zero volts, while the forward voltage required to drive various current densities $J = 10^{-8}, 10^{-7}, 10^{-6}, 10^{-5}, 10^{-4}, 10^{-3}, 10^{-2}, 0.025, 0.05, 0.1, 0.2$ A/cm^2 is applied at the cathode. The hole quasi-Fermi level $E_{f,P}$ deviates significantly from its equilibrium value at high currents due to the large density of holes injected from the contact. (b) Energy band diagram, total charge density, and electric field distributions through the device with an applied bias of 0.06 and 0.62 V. At small voltages (also for reverse bias) the inorganic semiconductor has a depletion region resulting in a positive space charge (scaled by 10× for visibility) in the inorganic at the OI-HJ. Most of the depleted charge is accumulated in the anode (Q_a, scaled by 0.2×) at the anode/organic interface. This results in a large electric field (lower panel) in the organic, sweeping holes away from the OI-HJ. When the device is forward biased, electrons are accumulated in the inorganic at the OI-HJ, and a large density of holes are injected into the organic film resulting in space-charge effects. Note that the x axis is scaled by 0.1× in the inorganic.

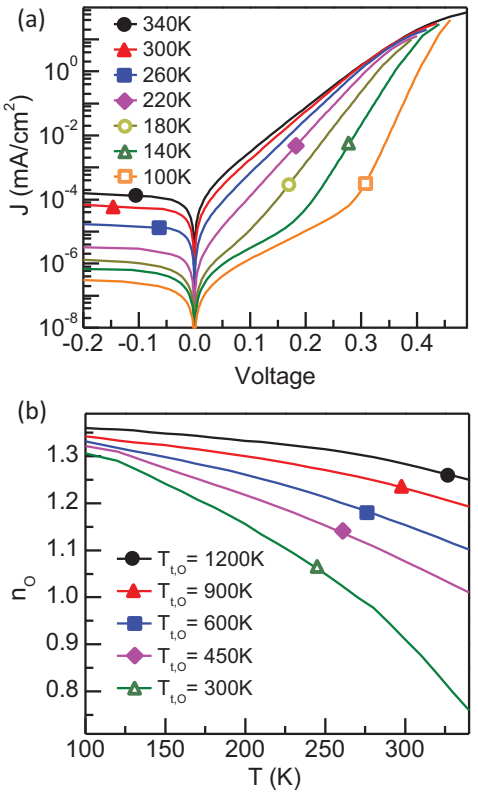

FIG. 6. (Color online) (a) Current density versus voltage J-V characteristics of the device in Fig. 4(a). Here, an exponential density of traps is assumed for both the organic and inorganic layer resulting in two exponential regions that are apparent at low temperature. Calculations based on a pentacene/Si device with material properties given in Table II. (b) The variation in ideality factor n_O as a function of temperature with different characteristic trap temperatures $T_{t,O}$ for the organic layer.

(or built-in) field. The small HCTE binding energy and large inorganic carrier mobility make the OI interface an efficient site for charge dissociation. Hence, it is useful for photocurrent generation in such devices as dye-sensitized solar cells [16] and as inter-element charge generating layers in stacked OLEDs [27] and tandem OPVs [28]. Furthermore, the OI interface can be used to efficiently generate photocurrent originating in organic layers by dissociating the tightly bound excitons produced following photon absorption.

Similar to excitonic photovoltaic junctions, losses in an OI-HJ solar cell [15] are incurred when HCTE dissociation is inefficient (i.e. $\eta_d < 1$). This occurs when there is strong interface recombination (i.e. R large). However, in the OI-HJ solar cell, η_d only affects the organic contribution to the photocurrent (viz. $J_{\rm ph} = q\eta_d J_X - J_I$), and this results in a loss in fill-factor [5] (FF). Figure 8(a) shows the dependence of FF on R for various trap temperatures in the organic. In all cases, HCTE dissociation is efficient when R is small resulting in a high FF. However, when R becomes large (i.e. $k_r \rightarrow k_d$), FF decreases due to enhanced interface recombination. This FF loss is more pronounced when $T_{t,O}$ is large due to the increase in midgap states available to enhance interface recombination.

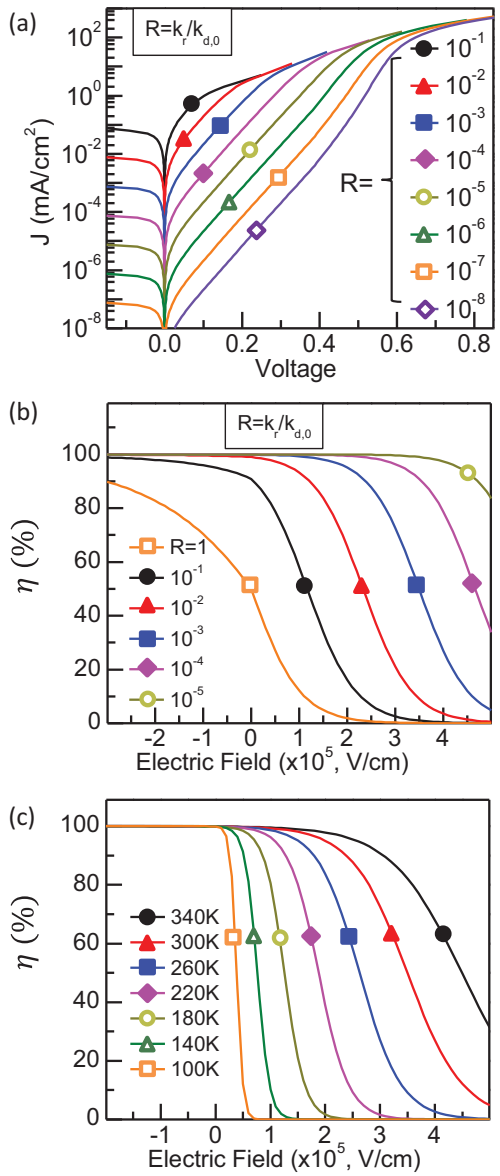

FIG. 7. (Color online) (a) Simulated device characteristics for various interface recombination rate ratios $R = k_r/k_{d,0}$, where $k_{d,0}$ is the HCTE state dissociation rate at zero electric field. (b) The efficiency of HCTE dissociation $\eta_d = k_d/(k_r + k_d)$ as a function of electric field and R. For most values of R, the dissociation is efficient when the electric field is less than zero. (c) HCTE dissociation efficiency versus electric field and temperature. At high temperature, η_d is large even for electric fields greater than zero.

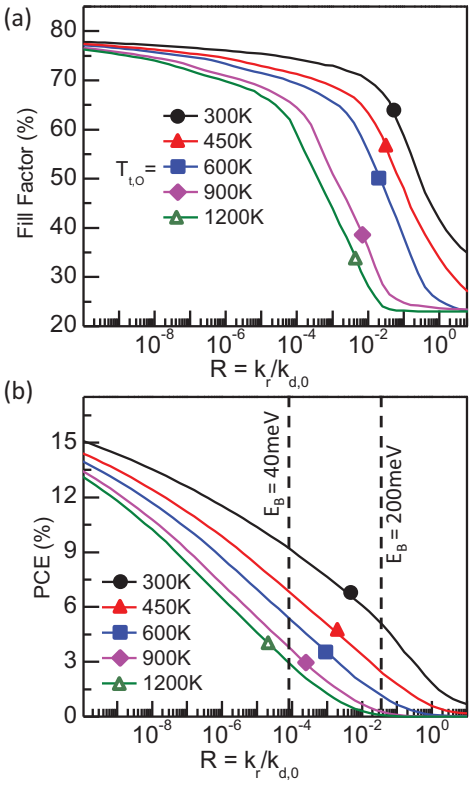

FIG. 8. (Color online) (a) Dependence of fill-factor FF on the ratio $R = k_r/k_{d,0}$ of the OI-HJ in Fig. 7, where k_r is the recombination rate of the HCTE and $k_{d,0}$ is its dissociation rate at zero electric field. Here, FF is plotted for various characteristic temperatures of the trap distribution in the organic layer $T_{t,O}$. In all cases, the FF is reduced when $R \rightarrow$ large due to enhanced HCTE recombination. (b) The power conversion efficiency PCE of the OI-HJ in Fig. 4 as a function of R for various $T_{t,O}$. The PCE increases with reduced R due to the increased FF and increased open-circuit voltage [c.f. Eq. (29)]. Vertical lines show values of R corresponding to HCTE binding energies $E_B = 40$ and 200 meV for $k_r = 10^9$ s^{-1}.

Now V_{OC} [see Eq. (32)] is also reduced with increasing R [c.f. Eq. (29)]. Since the solar cell power conversion efficiency (PCE) is given by $PCE = FF \times V_{OC} \times J_{SC}/P_{OPT}$, where J_{SC} is the short-circuit current and P_{OPT} is the incident optical power, then the trends in PCE closely follow those of V_{OC}, and to a lesser extent FF. As a result, PCE is also reduced with increasing R, as shown in Fig. 8(b). In calculating PCE, we have assumed 60% external quantum efficiency at a monochromatic incident illumination wavelength of 650 nm. Note that an accurate calculation of V_{OC} and PCE requires consideration of response across the entire solar spectrum and the corresponding optical absorption model [59,60] at each wavelength.

Throughout this treatment, we have assumed that the contact barrier at the anode ϕ_O is constant. In fact, its value is determined by the difference in anode work function and the HOMO level if the work function lies within the organic energy gap. Interface dipoles commonly observed at the organic/metal interface, however, will result in a corresponding shift in ϕ_O [61]. As shown by Greiner *et al.* [62], a large work function energy may result in Fermi level pinning at a few tenths of an electron volt above the organic HOMO. We expect this to be the case at small J, where ϕ_O is determined by the energy level alignment between the anode and the organic. We show in Paper II [34] that this assumption may not be valid at high currents, particularly when the OI-HJ is in the space-charge regime, far from equilibrium.

Finally, we point out that exciton generation in the organic layer may not always result in photocurrent generation in the OI-HJ diode. For example, extremely rapid quenching of excitons by surface states at the inorganic interface, or a lack of resonance between energy levels on both sides of the

TABLE III. Comparison of diode equations.[a]

Equation	J_s	J_{ph}	χ	n
Inorganic (diffusion)	$q\left[\frac{D_p n_i^2}{L_p N_D}+\frac{D_n n_i^2}{L_n N_A}\right]$	J_I	1	1
Inorganic[b] (generation, recombination)	$\frac{q n_i}{\tau_t}\left(\frac{k_B T}{q}\frac{2\varepsilon}{qWN_D}\right)$	J_I	$\frac{W}{\left(\frac{k_B T}{q}\frac{2\varepsilon}{qWN_D}\right)}$	2
Organic	$qa_0 k_{\text{rec}} N_{\text{HOMO}} N_{\text{LUMO}}(1-\eta_{PPd})\exp\left(-\frac{\Delta E_{\text{HL}}}{k_B T}\right)$	$\eta_{PPd} J_X$	$\frac{k_{PPd}}{k_{PPd,\text{eq}}}$[c]	$n_A=\frac{l_A}{\delta_D(l_A-1)+1}$
Hybrid	$q\langle a\rangle k_{\text{rec}} N_{\text{HOMO}} N_c(1-\eta_d)\exp\left(-\frac{\Delta E_{\text{OI}}}{k_B T}\right)$	$\eta_d J_O + J_I$	$\frac{k_d}{k_{d,\text{eq}}}$[c]	$n_O=\frac{l_O}{\delta_I(l_O-1)+1}$

[a]Only one-sided junctions are considered here. Generalizations of these expressions to more complex situations (e.g. double sided junctions) are found in this paper, Ref. [2], and in the vast literature on inorganic semiconductor diodes.
[b]This considers the simplest case of Shockley-Read-Hall recombination via a single midgap trap level in a symmetric *p-n* homojunction with $N_C = N_V$, $N_D = N_A$, and $|V_a| \gg k_B T/q$.
[c]Here, $k_{ppd} = k_{ppd,\text{eq}}$ and $k_d = k_{d,\text{eq}}$ at $V = 0$.

HJ that promote dissociation of the HCTE, can significantly reduce the photocurrent contribution from the organic layer. Indeed, in Paper II, we will show that although significant photogeneration from the organic occurs in wide band gap TiO_2-based junctions, this phenomenon is only observed at low temperatures (where surface states are filled) when the much narrower band gap InP is used. Hence, which material combinations are optimal for exciton transport to and dissociation at organic/inorganic junctions remain an open question.

C. Universal ideal diode behavior

The ideal diode equation for hybrid OI-HJ devices [c.f. Eq. (13)] resembles the diode equation for an excitonic (i.e. organic) heterojunction given in Ref. [2]. Indeed, it is also similar to the diode equation for an inorganic *p-n* junction—whether it is governed by drift and diffusion processes (i.e. the Shockley equation in Ref. [1]) or by Shockley-Read-Hall generation and recombination statistics [63,64]. Across all of these systems, the diode equation has the universal functional form given by

$$J = J_s\left[\exp\left(\frac{qV}{nk_B T}\right)-\chi(V)\right]-J_{\text{ph}}. \tag{33}$$

Here, the saturation current density J_s, the ideality factor n, the bias-dependent reverse-bias factor $\chi(V)$, where $\chi(0)\rightarrow 1$, and the photocurrent J_{ph} have different functional forms in the various material systems due to the different physical processes that govern current at the junction. The definition of these parameters for each material system for one-sided junctions (i.e. where current is controlled by only one of the two contacting materials) are listed in Table III.

The universal form of the diode equation originates with the commonality of the fundamental physics at play in all of these material systems. The splitting of quasi-Fermi levels and Boltzmann statistics govern the free carrier distribution and result in an exponential current response to an applied voltage. The nonequilibrium condition imposed by the applied bias is sustained by a balance between carrier generation and recombination, even in the case of the Shockley junction where carrier recombination and generation occur in the neutral region rather than the transition region at the junction. The primary distinguishing feature of these junctions is the specific physics at play in the generation and recombination processes.

IV. CONCLUSIONS

We have presented a comprehensive, first-principles model for both energy (i.e. exciton) and charge transport dynamics at hybrid organic-inorganic heterojunctions. This model couples the descriptions of the current-limiting processes at the interface with the charge distribution across the entire structure. The model is characterized by a significant asymmetry in material properties between the contacting materials. The primary outcome of our analysis is the derivation of an ideal diode equation that describes the current-voltage relationship of junctions in the presence or absence of interface trap states. A new quasiparticle, the hybrid charge transfer exciton, whose properties are determined by the characteristics of both the organic and inorganic materials, is found to transfer energy from across the interface. This state is often unstable or only briefly stable at room temperature (compared to the Frenkel or charge transfer species characteristic of fully excitonic junctions) and hence provides efficient transfer of energy as is often observed in photonic devices such as dye sensitized solar cells, stacked OLEDs, and OPVs.

Our model can be used to accurately simulate OI-HJ device behavior such as *J-V* and capacitance-voltage characteristics. The model can be used to identify physical processes that dominate in the dynamical properties of the HJ. In the subsequent Paper II [34], we apply the model to understand thin-film hybrid OI-HJs and find that the relatively low hole mobilities in the organic layer as compared to the charge mobilities in the inorganic semiconductor result in an inflection in the fourth quadrant of the *J-V* characteristics. This model can be used to understand photocurrent generation processes

at the OI interface including the binding energy of a HCTE state.

ACKNOWLEDGMENTS

This paper was supported in part by Department of Energy, Office of Basic Energy Sciences as part of Energy Frontier Research Centers: The Center for Solar and Thermal Energy Conversion at the University of Michigan (award DE-SC000957, CKR, analysis and modeling) and the Air Force Office of Scientific Research (SRF, analysis). S.R.F. thanks The Technion, Israel Institute of Technology for providing support via a Lady Davis Visiting Professorship. We thank R. Krasny for helpful discussions.

APPENDIX

The model discussed above was developed to describe an n-P junction dominated by interfacial recombination according to the scheme of Fig. 1. It is straightforward to modify the model to describe other hybrid device architectures. Figure 9(a) shows the case of a Type-II n-P junction [5] with a small valence band offset ΔE_v such that current is dominated by injection from the organic HOMO into the inorganic valence band under forward bias. Carrier hopping in the organic (rather than band transport in the inorganic) suggests that the injection rate for a single carrier can be described by $k_{\rm hop} = v\exp(-\Delta E_v/k_BT)$ [6], where v is the hopping attempt frequency. The forward bias current is then given by $J = qa_O P_{\rm HJ} k_{\rm hop}$. Under reverse bias, the current is limited by Shockley-Read-Hall (SRH) generation in the depletion region or by minority carrier diffusion from the inorganic bulk. The current for this OI-HJ device is thus given by

$$J = \upsilon q a_O P_c \exp\left(\frac{qV_a - \Delta E_v}{nk_BT}\right) - \frac{qn_i W_D}{\tau} - q\sqrt{\frac{D_I}{\tau_I}}\frac{n_i^2}{N_D}. \tag{A1}$$

Here, we have used Eq. (6) for $P_{\rm HJ}$. The intrinsic carrier density is $n_i = \sqrt{N_c N_v}\exp(-E_{g,I}/2k_BT)$, τ_g is the SRH generation rate, $W_D = \sqrt{2\varepsilon_I V_I/qN_D}$ is the depletion width, D_I is the minority carrier diffusion length, τ_I is the minority carrier lifetime, and N_D is the ionized dopant density in the inorganic.

Figure 9(b) shows a Type-I n-N junction [5], where current is limited by electron injection over the conduction band discontinuity ΔE_c at the interface under forward bias. This injection corresponds to thermionic emission into the organic from the inorganic. Assuming an ohmic contact at the anode/organic interface, the reverse bias current is limited by transport through the organic film. The resulting current is given by

$$J = A^*T^2\exp\left(-\frac{\Delta E_c}{k_BT}\right)\exp\left(\frac{qV_I}{n_I k_BT}\right) - f(V_O), \tag{A2}$$

where A^* is the effective Richardson constant [5]. Here, $f(V_O) = q\mu_O N V_O/W_O$ at low currents when ohmic conduction is dominant in the organic. In this case, N is the electron (i.e. negative polaron) density in the organic and is generally a function of position. At high bias and current densities, the current is limited by space-charge conduction where $f(V_O) = 9\varepsilon_O\mu_O V_O^2/8W_O^3$ in the absence of traps or by trap-charge limited conduction in the presence of a large trap density where [50]

$$f(V_O) = N_{\rm LUMO}\mu_O q^{1-l_O}\left[\frac{\varepsilon_O l_O}{H_O(l_O+1)}\right]^{l_O} \times \left(\frac{2l_O+1}{l_O+1}\right)^{l_O+1}\frac{V_O^{l_O+1}}{W_O^{2l_O+1}}. \tag{A3}$$

In each of these cases, the current is coupled to charge transport as discussed in Sec. II.B. This determines the voltage distributions V_O and V_I required to evaluate current density as a function of the applied voltage $V_a = V_O + V_I$. Under forward bias, both devices in Figs. 9(a) and 9(b) behave as diodes (exhibiting exponential dependence of J versus V), but the reverse (or leakage) characteristics deviate from a traditional Shockley diode behavior.

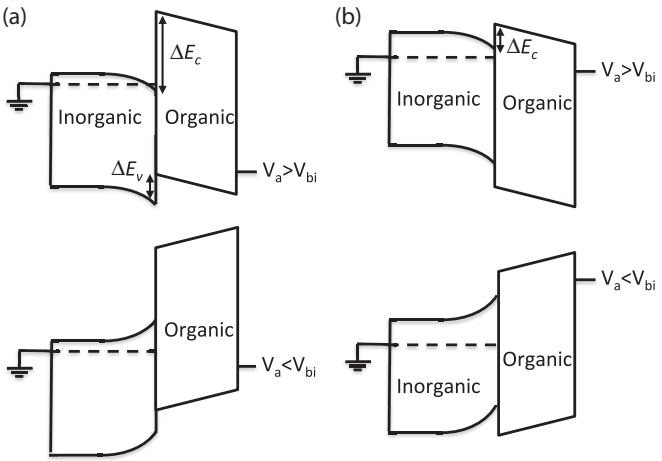

FIG. 9. (a) Alternative current conduction pathways for a type-II n-P organic/inorganic heterojunction (OI-HJ) when the HOMO to valence band discontinuity ΔE_v is small. Upon large forward bias (applied voltage is greater than the built-in voltage $V_a > V_{\rm bi}$), holes are injected as minority carriers into the inorganic valence band from the organic HOMO. These minority carriers ultimately recombine with free electrons. Upon reverse bias or moderate forward bias $V_a < V_{\rm bi}$, the current is dominated by Shockley-Read-Hall generation in the depletion region or minority carrier diffusion in the inorganic. (b) Current conduction pathway for a type-I n-N OI-HJ. Here, the forward bias current is limited by thermionic emission into the organic from the inorganic over the conduction band discontinuity (ΔE_c). Assuming an ohmic contact at the anode/organic interface, the reverse bias current is simply limited by drift or space charge current in the organic layer.

[1] W. Shockley, Bell Syst. Tech. J. **28**, 435 (1949).
[2] N. Giebink, G. Wiederrecht, M. Wasielewski, and S. Forrest, Phys. Rev. B **82**, 155305 (2010).
[3] N. Giebink, B. Lassiter, G. Wiederrecht, M. Wasielewski, and S. Forrest, Phys. Rev. B **82**, 155306 (2010).
[4] S. R. Forrest, Nature **428**, 911 (2004).
[5] S. M. Sze and K. K. Ng, *Physics of Semiconductor Devices*, 3rd ed. (Wiley, Hoboken, NJ, 2007).
[6] H. Bässler, Phys. Status Solidi B **175**, 15 (1993).
[7] S. F. Nelson, Y.-Y. Lin, D. J. Gundlach, and T. N. Jackson, Appl. Phys. Lett. **72**, 1854 (1998).
[8] D. Y. Zang, F. F. So, and S. R. Forrest, Appl. Phys. Lett. **59**, 823 (1991).
[9] R. C. Haddon, A. F. Hebard, M. J. Rosseinsky, D. W. Murphy, S. J. Duclos, K. B. Lyons, B. Miller, J. M. Rosamilia, R. M. Fleming, A. R. Kortan, S. H. Glarum, A. V. Makhija, A. J. Muller, R. H. Eick, S. M. Zahurak, R. Tycko, G. Dabbagh, and F. A. Thiel, Nature **350**, 320 (1991).
[10] J. Blochwitz, T. Fritz, M. Pfeiffer, K. Leo, D. M. Alloway, P. A. Lee, and N. R. Armstrong, Org. Electron. **2**, 97 (2001).
[11] M. Pope and C. E. Swenberg, *Electronic Processes in Organic Crystals and Polymers* (Oxford University Press, New York, 1999).
[12] N. W. Ashcroft and D. N. Mermin, *Solid State Physics*, 1st ed. (Cornell University, Ithaca, NY, 1976).
[13] F. F. So and S. R. Forrest, IEEE Trans. Electron Devices **36**, 66 (1989).
[14] S. R. Forrest and F. F. So, J. Appl. Phys. **64**, 399 (1988).
[15] N. Li, K. Lee, C. K. Renshaw, X. Xiao, and S. R. Forrest, Appl. Phys. Lett. **98**, 053504 (2011).
[16] N. Vlachopoulos, P. Liska, J. Augustynski, and M. Graetzel, J. Am. Chem. Soc. **110**, 1216 (1988).
[17] A. Hagfeldt, G. Boschloo, L. Sun, L. Kloo, and H. Pettersson, Chem. Rev. **110**, 6595 (2010).
[18] E. H. Sargent, Nat. Photonics **6**, 133 (2012).
[19] S. A. Mcdonald, G. Konstantatos, S. Zhang, P. W. Cyr, E. J. Klem, L. Levina, and E. H. Sargent, Nat. Mater. **4**, 138 (2005).
[20] S. Coe-Sullivan, W.-K. Woo, J. S. Steckel, M. Bawendi, and V. Bulović, Org. Electron. **4**, 123 (2003).
[21] W. U. Huynh, Science **295**, 2425 (2002).
[22] V. M. Agranovich, Y. N. Gartstein, and M. Litinskaya, Chem. Rev. **111**, 5179 (2011).
[23] J. Wenus, R. Parashkov, S. Ceccarelli, A. Brehier, J.-S. Lauret, M. S. Skolnick, E. Deleporte, and D. G. Lidzey, Phys. Rev. B **74**, 235212 (2006).
[24] M. Slootsky, X. Liu, V. M. Menon, and S. R. Forrest, Phys. Rev. Lett. **112**, 076401 (2014).
[25] R. J. Holmes, S. Kéna-Cohen, V. M. Menon, and S. R. Forrest, Phys. Rev. B **74**, 235211 (2006).
[26] M. Kröger, S. Hamwi, J. Meyer, T. Riedl, W. Kowalsky, and A. Kahn, Appl. Phys. Lett. **95**, 123301 (2009).
[27] X. Qi, N. Li, and S. R. Forrest, J. Appl. Phys. **107**, 014514 (2010).
[28] B. E. Lassiter, J. D. Zimmerman, A. Panda, X. Xiao, and S. R. Forrest, Appl. Phys. Lett. **101**, 063303 (2012).
[29] S. R. Forrest, M. L. Kaplan, and P. H. Schmidt, J. Appl. Phys. **55**, 1492 (1984).
[30] S. R. Forrest, M. L. Kaplan, and P. H. Schmidt, J. Appl. Phys. **56**, 543 (1984).
[31] S. R. Forrest, M. L. Kaplan, P. H. Schmidt, W. L. Feldmann, and E. Yanowski, Appl. Phys. Lett. **41**, 90 (1982).
[32] H. Méndez, I. Thurzo, and D. R. T. Zahn, Phys. Rev. B **75**, 045321 (2007).
[33] S. R. Forrest, M. L. Kaplan, P. H. Schmidt, and J. M. Parsey, J. Appl. Phys. **58**, 867 (1985).
[34] A. Panda, C. K. Renshaw, A. Oskooi, K. Lee, and S. R. Forrest, Phys. Rev. B **90**, 045303 (2014).
[35] A. Yella, H.-W. Lee, H. N. Tsao, C. Yi, A. K. Chandiran, M. K. Nazeeruddin, E. W.-G. Diau, C.-Y. Yeh, S. M. Zakeeruddin, and M. Grätzel, Science **334**, 629 (2011).
[36] X. Xiao, J. D. Zimmerman, B.E. Lassiter, K. J. Bergemann, and S. R. Forrest, Appl. Phys. Lett. **102**, 073302 (2013).
[37] S. Avasthi, Y. Qi, G. K. Vertelov, J. Schwartz, A. Kahn, and J. C. Sturm, Appl. Phys. Lett. **96**, 222109 (2010).
[38] A. B. Sieval, C. L. Huisman, A. Schönecker, F. M. Schuurmans, A. S. H. van der Heide, A. Goossens, W. C. Sinke, H. Zuilhof, and E. J. R. Sudhölter, J. Phys. Chem. B **107**, 6846 (2003).
[39] I. Haeldermans, K. Vandewal, W. D. Oosterbaan, A. Gadisa, J. D'Haen, M. K. V. Bael, J. V. Manca, and J. Mullens, Appl. Phys. Lett. **93**, 223302 (2008).
[40] Y. Vaynzof, A. A. Bakulin, S. Gélinas, and R. H. Friend, Phys. Rev. Lett. **108**, 246605 (2012).
[41] N. Bansal, L. X. Reynolds, A. MacLachlan, T. Lutz, R. S. Ashraf, W. Zhang, C. B. Nielsen, I. McCulloch, D. G. Rebois, T. Kirchartz, M. S. Hill, K. C. Molloy, J. Nelson, and S. A. Haque, Sci. Rep. **3**, 1531 (2013).
[42] L. Onsager, J. Chem. Phys. **2**, 599 (1934).
[43] G. H. Wannier, Phys. Rev. **52**, 191 (1937).
[44] F. F. So and S. R. Forrest, Phys. Rev. Lett. **66**, 2649 (1991).
[45] R. J. Fleming, J. Chem. Phys. **56**, 4911 (1972).
[46] G. A. de Wijs, C. C. Mattheus, R. A. de Groot, and T. Palstra, Synth. Met. **139**, 109 (2003).
[47] C. L. Braun, J. Chem. Phys. **80**, 4157 (1984).
[48] P. Debye, Trans. Electrochem. Soc. **82**, 265 (1942).
[49] T. Chasse, C.-I. Wu, I. G. Hill, and A. Kahn, J. Appl. Phys. **85**, 6589 (1999).
[50] P. Mark and W. Helfrich, J. Appl. Phys. **33**, 205 (1962).
[51] J. van de Lagemaat and A. J. Frank, J. Phys. Chem. B **104**, 4292 (2000).
[52] S. Hirae, M. Hirose, and Y. Osaka, J. Appl. Phys. **51**, 1043 (1980).
[53] L. M. Peter, J. Li, and R. Peat, J. Electroanal. Chem. Interfacial Electrochem. **165**, 29 (1984).
[54] N. F. Mott and R. W. Gurney, *Electronic Processes in Ionic Crystals*, 1st ed. (Clarendon Press, Oxford, 1940).
[55] B. Lüssem, M. Riede, and K. Leo, Phys. Status Solidi A **210**, 9 (2013).
[56] J. Kido and T. Matsumoto, Appl. Phys. Lett. **73**, 2866 (1998).
[57] T. D. Anthopoulos and T. S. Shafai, Appl. Phys. Lett. **82**, 1628 (2003).
[58] J. Schafferhans, A. Baumann, A. Wagenpfahl, C. Deibel, and V. Dyakonov, Org. Electron. **11**, 1693 (2010).
[59] L. A. Pettersson, L. S. Roman, and O. Inganas, J. Appl. Phys. **86**, 487 (1999).
[60] P. Peumans, A. Yakimov, and S. R. Forrest, J. Appl. Phys. **93**, 3693 (2003).

[61] J. Hwang, A. Wan, and A. Kahn, Mater. Sci. Eng. R Rep. **64**, 1 (2009).

[62] M. T. Greiner, M. G. Helander, W.-M. Tang, Z.-B. Wang, J. Qiu, and Z.-H. Lu, Nat. Mater. **11**, 76 (2011).

[63] W. Shockley and W. T. Read, Phys. Rev. **87**, 835 (1952).

[64] C.-T. Sah, R. N. Noyce, and W. Shockley, Proc. IRE **45**, 1228 (1957).